

JOURNAL OF SCIENCE



SAKARYA UNIVERSITY

Sakarya University Journal of Science

ISSN 1301-4048 | e-ISSN 2147-835X | Period Bimonthly | Founded: 1997 | Publisher Sakarya University |
<http://www.saujs.sakarya.edu.tr/>

Title: Numerical Investigation of Incompressible Forced Convection in a Channel with a Rectangular Prism

Authors: Mert Özsaban, Erman Aslan, Hasan Rıza Güven

Received: 2019-04-09 18:53:59

Accepted: 2019-07-04 10:50:19

Article Type: Research Article

Volume: 24

Issue: 1

Month: February

Year: 2020

Pages: 10-18

How to cite

Mert Özsaban, Erman Aslan, Hasan Rıza Güven; (2020), Numerical Investigation of Incompressible Forced Convection in a Channel with a Rectangular Prism. Sakarya University Journal of Science, 24(1), 10-18, DOI: 10.16984/saufenbilder.551492

Access link

<http://www.saujs.sakarya.edu.tr/tr/issue/49430//551492>

New submission to SAUJS

<http://dergipark.gov.tr/journal/1115/submission/start>



Numerical Investigation of Incompressible Forced Convection in a Channel with a Rectangular Prism

Mert Özşaban^{*1}, Erman Aslan², Hasan Rıza Güven³

Abstract

The aim of the present study is to investigate the effects of the rectangular prism on forced convection in a channel with the Lattice Boltzmann Method (LBM). In this context, numerical analysis of steady and unsteady incompressible flow and heat transfer has been done in a two-dimensional straight parallel channel. Momentum and energy transport are modelled with LBM. This study is used as a single relaxation time rule with a uniform square lattice structure. Different Reynolds numbers (50 and 1000) and constant Prandtl number value (0.7) have been investigated. In this study Nusselt number has been calculated for channel flow with rectangular prism and it was compared with an empty channel. Streamlines and isotherms were presented for the above-mentioned cases. LBM results were validated by commercial CFD code with the same conditions. It is found from results that Nusselt number with a rectangular prism in a channel was increased and the flow goes to transient form at $Re=1000$. Also, LBM code results are similar accuracy with commercial CFD code.

Keywords: Lattice Boltzmann Method, Nusselt number, incompressible forced convection, rectangular prism

1. INTRODUCTION

Lattice Boltzmann Method (LBM) can provide a faster solution than traditional CFD methods as Finite Difference Method and Finite Volume Method but it needs more memory [1]. In traditional CFD methods, nonlinear partial differential equations are converted to non-linear

algebraic equations and these equations are solved by iterations [2]. In the Lattice Boltzmann Method, the Navier-Stokes equation is approximately solved by colliding and advancing the fluid particles according to their lattice structure. LBM [2-4] relies upon a lattice structure that is orthogonal and equidistant. Staircase

¹ Recep Tayyip Erdogan University, Department of Mechanical Engineering, Rize, Turkey.
ORCID: 0000-0001-6818-6428

² Istanbul University-Cerahpaşa, Department of Mechanical Engineering, İstanbul, Turkey.
ORCID: 0000-0001-8595-6092

³ Istanbul University-Cerahpaşa, Department of Mechanical Engineering, İstanbul, Turkey.
ORCID: 0000-0002-0820-4927

boundary and “bounce-back” wall boundary conditions are widely used [5, 6].

Liu et al. [7] studied the bluff body especially on a circular cylinder in a channel flow. They have computed the turbulence energy at high Reynolds number and validate results from experimental data.

Prosser and Smith [8] studied the various range of angle of attack on the rectangular bluff body. They present lift curved and modelled lift angle.

Joubert et al. [9] studied the turbulent flow of various shapes of a rectangular prism in a wind tunnel and computational simulation in three-dimensional. They used the model of simulation turbulence Spalart – Allmaras enhanced delayed detached eddy simulation (IDDES). They compared results with time-averaged experimental data from particle image velocimetry at high Reynolds number.

Teixeira et al. [10] studied turbulent flow with force convection of various dimensions arrangements of the three-square prism in two-dimensional. They have worked on Nusselt number velocity profiles and drag coefficient. They are modelled turbulence flow with RANS *SST – k- ω* and they solve time-averaged conservation equations with Finite Volumes Method.

Cimarelli et al. [11] have worked on 1/5 rectangular prism at 3000 Reynold number. They solved their problem with direct numerical simulation of the finite volume method. They presented drag and lift coefficient, mean velocity fields and turbulent kinetic energy.

Kawamura et al. [12] studied heat transfer in the turbulent and transient flow of rectangular prism in a channel. They solved the problem by direct numerical simulation in three-dimensional. They presented in their study time-averaged vortex structure and the local Nusselt number for various Reynolds number. They compared the results of the Nusselt number and friction factor with experimental data.

Rossinelli et al. [13] studied bluff bodies especially on a circular cylinder in two-dimensional. They compared CPU and GPU accelerated solver results. They presented drag and lift coefficients, vorticity contour with different low and medium Reynolds numbers (40-9500) from CPU and GPU solver results.

The novelty of this study is investigating a rectangular prism in the channel flow with the Lattice Boltzmann Method (LBM) to the analysis of the velocity and heat transfer. The study presents 2D LBM code results for benchmark transport of thermal energy, incompressible steady-state and unsteady flows for two different Reynolds number (50, 1000) and constant Prandtl number (0.7). LBM results compared with a commercial CFD code [14]. Computational time and heat transfer accuracy compared with LBM code and commercial CFD code each other. Lattice Boltzmann Method examines the similar problem of forced convection in a rectangular obstacle channel [15-17]. Two studies [15,16] modelled just flow equation by LBM and one study [17] modelled flow equation by LBM and modelled energy equation by finite difference method. In this study momentum and energy equations computed by LBM.

2. PROBLEM DEFINITION

Figure 1 shows the sketch of the problem geometry. In Figure 1, the rectangular prism in the middle of the channel. At the north and south walls, boundary conditions are no-slip boundary conditions; x-velocity (u)=0 and y-velocity (v)=0 for momentum equations. For the energy equation at the north and south walls is prescribed constant temperature (T)=0 and at the rectangular prism (RP) adiabatic wall is assumed. Inlet velocity boundary type is constant over the y-axis ($u=u_0$), $v=0$ and $T=0$. At the outlet of the channel, constant static pressure is prescribed for momentum equation and zero-gradient boundary conditions for energy equations. In this study, low and medium Reynolds numbers (Re) have been studied. In the solution of medium Reynolds number exhibits longer vortex shedding than low Re.

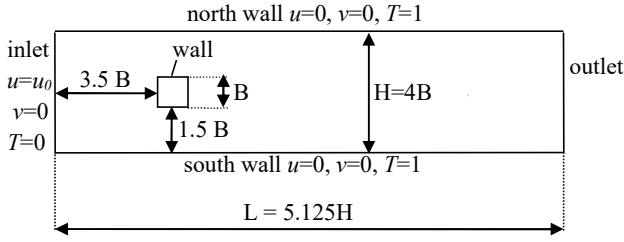


Figure 1. Domain and boundary types of channel flow with the rectangular prism

3. MATHEMATICAL AND NUMERICAL FORMULATION

LBM formulations are generally used in literature by a single Bhatnagar - Gross - Krook (BGK) relaxation time approximation [18]. A BGK [19] version is adopted in this study. This version is appropriate for incompressible unsteady flows. In the present study shown in Figure 2, the two-dimensional (2D) and nine velocity model of LBM (D2Q9) is used. In the present work, the single time relaxation and square lattice structures have been used.

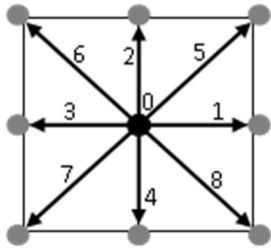


Figure 2. LBM D2Q9 lattice model

Distribution functions in the collision step for momentum and streaming transport are shown below [2];

$$\tilde{f}_\alpha(\vec{x}, t + \Delta t) = f_\alpha(\vec{x}, t) - \omega \left[f_\alpha(\vec{x}, t) - f_\alpha^{eq}(\vec{x}, t) \right] \quad (1)$$

$$\tilde{g}_\alpha(\vec{x}, t + \Delta t) = g_\alpha(\vec{x}, t) - \omega_T \left[g_\alpha(\vec{x}, t) - g_\alpha^{eq}(\vec{x}, t) \right] \quad (2)$$

In Equation 1 and Equation 2, t is the time and \vec{x} is the position vector.

Distribution functions in the streaming step for momentum and streaming transport are provided below;

$$f_\alpha(\vec{x} + \vec{c}_\alpha \Delta t, t + \Delta t) = \tilde{f}_\alpha(\vec{x}, t + \Delta t) \quad (3)$$

$$g_\alpha(\vec{x} + \vec{c}_\alpha \Delta t, t + \Delta t) = \tilde{g}_\alpha(\vec{x}, t + \Delta t) \quad (4)$$

The momentum and energy equations of collision frequencies are obtained from below respectively;

$$\omega = \frac{1}{\frac{3\nu\Delta t}{\Delta x^2} + 0.5} \quad (5)$$

$$\omega_T = \frac{1}{\frac{3\alpha\Delta t}{\Delta x^2} + 0.5} \quad (6)$$

In Equation 5, ν is the dynamic viscosity and in Equation 6 α is the thermal diffusivity.

The lattice sound speed is shown as below,

$$c_s = \frac{c}{\sqrt{3}} \quad (7)$$

The lattice speed is defined as,

$$c = \frac{\Delta x}{\Delta t} \quad (8)$$

In the present study uniform (square) lattice has been used and time step equal to mesh. Therefore lattice speed is equal to one and lattice sound speed results by below,

$$c_s = \frac{1}{\sqrt{3}} \quad (9)$$

Two-dimensional nine discrete velocities are shown below in the matrix form,

$$\vec{c}_\alpha = c \begin{bmatrix} 0 & 1 & 0 & -1 & 0 & 1 & -1 & -1 & 1 \\ 0 & 0 & 1 & 0 & -1 & 1 & 1 & -1 & -1 \end{bmatrix} \quad (10)$$

The equilibrium distribution functions for momentum and energy transport are presented below;

$$f_\alpha^{eq} = w_\alpha \left[\rho + \frac{3}{c^2} \vec{c}_\alpha \cdot \vec{u} + \frac{9}{2c^4} (\vec{c}_\alpha \cdot \vec{u})^2 - \frac{3}{2c^2} \vec{u} \cdot \vec{u} \right] \quad (11)$$

$$g_{\alpha}^{eq} = w_{\alpha} T \left[1 + \frac{3}{c^2} \vec{c}_{\alpha} \cdot \vec{u} \right] \quad (12)$$

In Equation 11, ρ is the density and \vec{u} is the axial velocity vector. T is the temperature in Equation 12.

The weighting factors for all lattice directions are given as below,

$$w_{\alpha} = \begin{cases} \frac{4}{9} & \text{for } \alpha = 0 \\ \frac{1}{9} & \text{for } \alpha = 1, 2, 3, 4 \\ \frac{1}{36} & \text{for } \alpha = 5, 6, 7, 8 \end{cases} \quad (13)$$

The macroscopic fields that are given respectively by velocity (\vec{u}), temperature (T), density (ρ), pressure (p);

$$\vec{u} = \sum_{\alpha=0}^8 \vec{c}_{\alpha} f_{\alpha} = \sum_{\alpha=0}^8 \vec{c}_{\alpha} f_{\alpha}^{eq} \quad (14)$$

$$T = \sum_{\alpha=0}^8 g_{\alpha} = \sum_{\alpha=0}^8 g_{\alpha}^{eq} \quad (15)$$

$$\rho = \sum_{\alpha=0}^8 f_{\alpha} = \sum_{\alpha=0}^8 f_{\alpha}^{eq} \quad (16)$$

$$p = \sum_{\alpha=0}^8 p_{\alpha} = \sum_{\alpha=0}^8 p_{\alpha}^{eq} \quad (17)$$

$$p_{\alpha} = c_s^2 f_{\alpha} \quad (18)$$

$$p_{\alpha}^{eq} = c_s^2 f_{\alpha}^{eq} \quad (19)$$

The implementation of the boundary conditions in details is used from the literature [2, 3]. The bounce-back boundary condition is applied at walls.

4. RESULTS AND DISCUSSION

In the present study, all cases from both LBM and Fluent calculations are based on square-shape grids. LBM results obtained by a commercial

CFD code Ansys-Fluent [14] are utilized. In Fluent calculations, the second-order upwind scheme was used to discrete the convective terms. In addition, the SIMPLEC scheme is used for steady-state computation to treat the velocity-pressure coupling and the PISO algorithm [20] is used for unsteady computations in Fluent. In all Fluent calculations, the default values are used as 0.7 value of momentum and 1.0 value of the pressure for under-relaxation factors, 10^{-6} is taken for energy, continuity, x-velocity and y-velocity as the convergence criteria. For unsteady fluent calculations, a second order Implicit time integration scheme is applied [14]. LBM and Fluent computations have the same time step size for steady-state flows. In the unsteady flows, same time step size and time step size which is provide the Courant number (Co) less than or equal to one are both used in the study. For the unsteady calculations, time-averaged and time-invariant results are used.

4.1. Preliminary Validation

The presently developed LBM code is firstly validated for incompressible, steady-state, laminar flow. A comparison is conducted for this purpose with the analytical solution available in a fully-developed channel flow for the forced laminar convection. A simple channel geometry (without a rectangular prism) modelled with the constant inlet and wall temperature for $Re = 50$. Inlet value of temperature is “0” and the wall temperature is “1”. The length of the channel is defined to be sufficient to permit a fully developed thermal flow [21]. The Nusselt number predicted by LBM for the fully developed channel flow is compared with the theoretical value [21]. The agreement of both values confirms the accuracy of the present LBM code resulted in Table 1.

Table 1. Fully developed channel flow Nusselt number at $Re = 50$

	LBM code	Theory [21]
Nusselt Number	7.54	7.54

4.2. Predictions for Different Reynolds Numbers

Predictions are performed for $Re = 50$ and 1000 . In these computations, based on the full channel domain, a steady-state flow solution at $Re = 50$ ($dx=dt=0.5$, $mesh=32800$) is observed. For the higher number of Reynolds at $Re = 1000$, an unstable behaviour with vortex shedding is observed. In unsteady computations (LBM and Fluent), the time step size applied may be considered fairly small, resulting in a resolution of a period in at least 1461 time steps and in cell Courant numbers (Co) (Peyret, 1996) about 0.1 (based on the mean inlet velocity) in terms of the finite volume method. Also Results of $Co = 0.1(dx=dt=0.125, mesh= 537600)$ and $Co=0.8(dx=0.125, dt=1, mesh=537600)$ are compared with each other and LBM results.

4.2.1. Velocity Fields

Figure 3 shows LBM results of the streamlines of the unsteady/instantaneous and unsteady/time-averaged flow at $Re = 1000$, and the streamlines of the steady-state at $Re = 50$, at the rectangular prism zone.

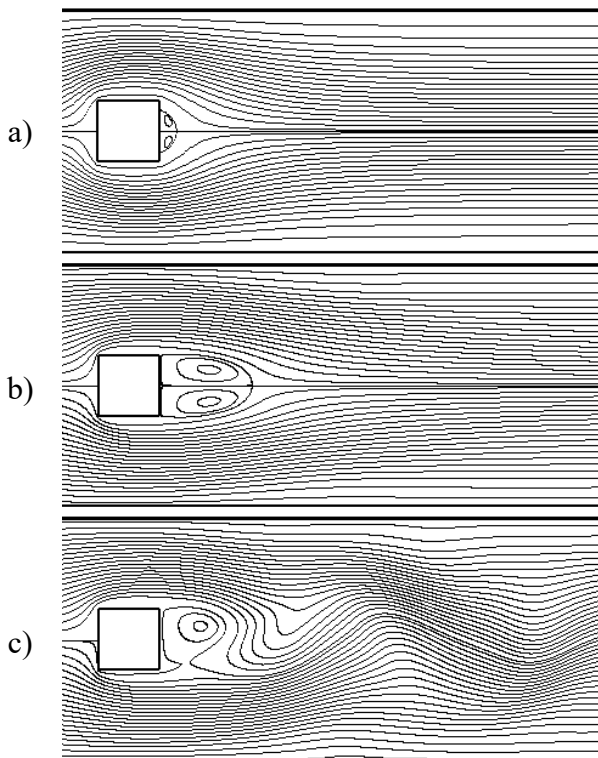


Figure 3. Streamlines predicted by LBM: (a) steady-state $Re = 50$, (b) unsteady/time-averaged $Re=1000$, and (c) unsteady/instantaneous $Re=1000$

The instantaneous streamlines indicate the unsteady flow structure behind the RP due to vortex shedding at any time (Figure 3c). At $Re = 50$, the time-averaged velocity field streamlines appear symmetrical and display a slight recirculation zone behind the prism (Figure 3a). The time-averaged unsteady flow at $Re = 1000$ exhibits high recirculation zone size (Figure 3b).

For the steady-state and unsteady time-averaged flow at $Re = 50$ and 1000 , Table 2 present the Drag coefficients (C_D) and Strouhal numbers (St) predicted by LBM and Fluent. Here, in determining the Strouhal number, the frequency related to the lifting force on the RP is considered.

Table 3 compares the length of the recirculation zone (nondimensionalized by B) behind the rectangular prism, predicted for different Reynolds numbers by different methods. They are steady-state at $Re = 50$, unsteady time-average and unsteady instantaneous at $Re = 1000$. Recirculation zone length at $Re = 1000$ bigger than at $Re = 50$. LBM and Fluent computation results are similar to each other.

Table 2. Drag coefficients (C_D) and Strouhal numbers (St) predicted for $Re = 50$ and 1000

	LBM	Fluent	% deviation
C_D (steady-state, $Re = 50$)	13.77	14.64	5.94 %
C_D (unsteady, $Re=1000$)	2.55	2.63	3.04 %
St (unsteady, $Re = 1000$)	2.15	2.19	1.83 %

Table 3. Recirculation zone length behind rectangular prism for different Re

	$Re=50$ (steady-state)	$Re=1000$ (unsteady/time-average)
LBM	0.276 B	1.519 B
Fluent	0.257 B	1.594 B
% derivation	7.39 %	4.70 %

LBM predicted isotherms for cases with and without rectangular prism are shown in Figure 4 using different modelling approaches at $Re = 50$ and 1000 . The steady-state solutions shown in Figures. 4a, 4b and 4c. Figure 4d and 4e present unsteady solutions. In Figure 4, the nondimensional temperature has the value "0" at the inlet and the value "1" on the walls, where the step size between the isotherms is 0.05.

The temperature field's unsteady/periodic pattern can be seen in Figure 4e. The unsteady solution's time-averaged results (Figure 4d) are different from the steady-state solution (Figure 4c) and mean a significant increase in heat transfer.

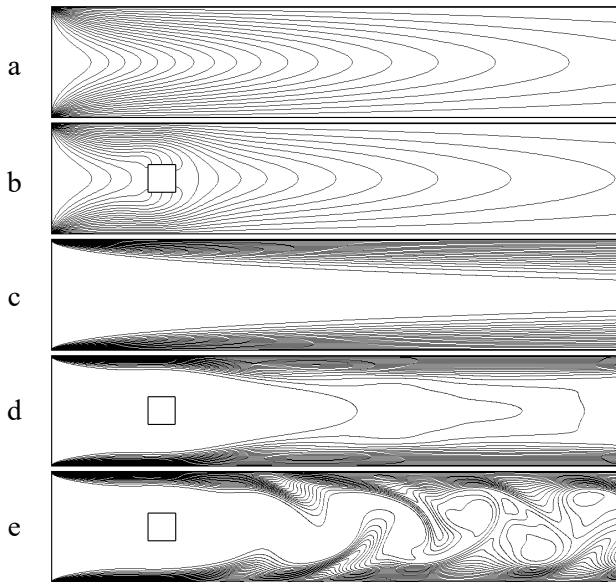


Figure 4. Temperature distribution predicted by LBM: (a) steady-state without prism $Re = 50$, (b) steady-state with prism $Re = 50$, (c) steady-state without prism $Re = 1000$ (d) unsteady/time-averaged with prism $Re=1000$, and (e) unsteady/instantaneous with prism $Re=1000$

4.2.2. Heat Transfer

Variations of the Nusselt number along the channel wall, predicted for $Re = 50$, are presented in Figure 5. One can observe that the rectangular prism causes an increase in the Nusselt number in a region near the prism ($0.1 < x/L < 0.3$). This is due to the increased near-wall velocities because of flow acceleration due to the blockage by the prism. The unsteady phenomena do not play any

role here, as a steady-state is predicted for this Reynolds number. One can see that the present LBM predictions agree very well with the Fluent predictions (Figure 5).

Variations of the Nusselt number along the channel wall predicted for $Re = 1000$ are presented in Figure 6. For this Reynolds number, the flow is unsteady/periodic. The Nusselt number increases around rectangular prism in the unsteady results, because of the increased skin friction by the blockage.

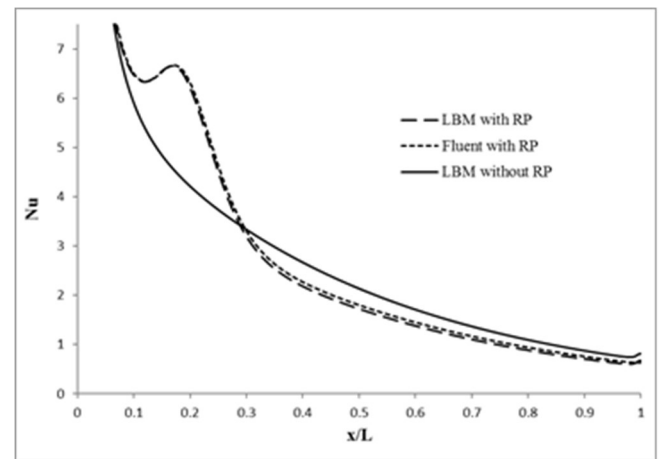


Figure 5. Nusselt number along the channel wall at $Re = 50$.

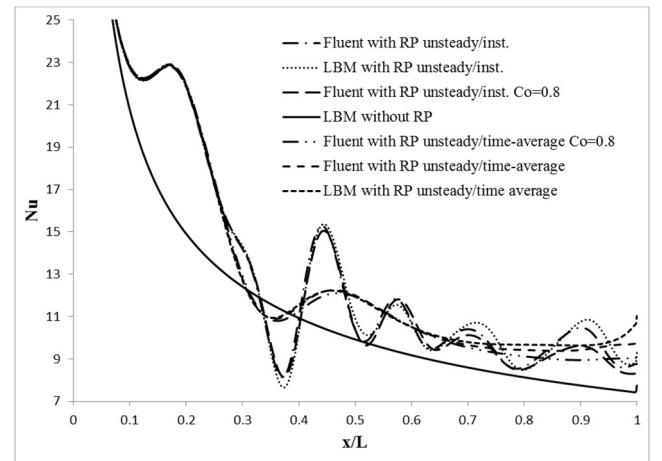


Figure 6. Nusselt number along the channel wall at $Re = 1000$.

However, behind the rectangular prism, Steady-state Nu forecasts undershoot the case's values without prism, since the near-wall flow (under steady-state assumptions) shows a region of deceleration behind prism. However, a higher

mean of Nusselt number value still forecasts. However, since the flow is unsteady/periodic, steady-state results artificially obtained that they do not have much physical importance (and can be quite inaccurate, as seen in the comparison). Figure 6 presents the variation of the Nusselt number for the instantaneous and the time-averaged flow. The time-averaged variation of the Nusselt number shows a local peak at nearly the same location as the stationary solution, but slightly lower. This is followed in the downstream by a secondary local peak. The time-averaged Nusselt numbers, especially in the downstream region, are much higher than those of the case without prism and those of the stationary computation with RP. Thus, one can see that a rectangular prism can enhance heat transfer to channel walls, and this effect is primarily due to the unsteady-periodic vortex shedding. LBM and Fluent results are found to be in accordance again.

Table 4 compares the CPU times required by LBM and Fluent, for computing a period of the case at $Re = 1000$. The cell Courant numbers are also indicated in the table. As already mentioned above, in the main computations, the time-step size has been chosen in such a way that the cell Courant number takes a value of about 0.1. Given the Reynolds number and the grid resolution, this value cannot arbitrarily be increased for LBM, due to stability considerations [2]. For better comparability, Fluent computations have also been carried out using the same time-step size, resulting in $Co = 0.2$. This comparison seems to be very much in favour of LBM (Table 4): the user time of LBM (304 s) is only 0.4% of the user time of Fluent (76,713 s). However, this picture is misleading, since the finite volume method does not have the same stability limitations as LBM, and Co can be larger for Fluent computations, without a principal loss of accuracy. Although the implicit backward time differencing applied in the Fluent computations does not have a theoretical stability limit, a time step corresponding to $Co \leq 1$ is generally assumed to be a safe upper limit for an accurate resolution of the physical unsteady phenomena.

Thus, Fluent computations have also been performed for $Co = 0.8$, assuming this value of Co

to be reasonably near the upper limit for an ideal accuracy in Fluent computations. As can be seen in Table 4, the user time of Fluent computations for $Co = 0.8$ is, of course, smaller than that of $Co = 0.1$. Comparing this computation (Fluent, $Co = 0.8$) with LBM, one can see that the user time of LBM (304 s) is only 3.3% of the user time of Fluent (9,108 s). This comparison is also quite in favour of LBM. Nevertheless, this is still not a fair comparison: The present LBM formulation is based on a square-shaped lattice structure. For keeping ideal comparability for the accuracy, the finite volume grids were also constructed in a practically identical manner. However, this was not necessary for the Fluent computations: rectangular shaped cells, expanding grids, etc. could be used in Fluent computations, without a principal loss of accuracy, which would result in a smaller number of grid nodes and smaller CPU times. On the other hand, the LBM grid could also be designed to be non-equidistant by using, e.g., various interpolation techniques which also would result in a coarser grid and smaller CPU times for LBM. Such techniques for LBM are planned to be considered within the next development stage of the present LBM code. Thus, a more conclusive and fair comparison of the CPU requirements is planned to be performed within the framework of the planned future work.

Table 4. CPU times (serial computing)

	LBM Co=0.1	Fluent Co=0.1	Fluent Co=0.8
Computation time (s)	304	76,713	9,108

5. CONCLUSIONS

The laminar forced convection is investigated computationally in a two-dimensional channel with an integrated rectangular prism by the Lattice Boltzmann Method. It is assumed that flow is incompressible and material properties are constant. The Lattice Boltzmann Method is used in a 2D channel with an integrated rectangular prism to computationally investigate the laminar forced convection. It is observed that the rectangular prism can enhance heat transfer, particularly for the high Reynolds numbers, where an unsteady/periodic flow vortex shedding appears to be the principle responsible

for this enhancement. Examinations with an entrenched commercial CFD code approve the developed LBM code.

6. REFERENCES

- [1] M. H. H. Ishak, M. Z. Abdullah and A. Abas, “Lattice Boltzmann method study of effect three dimensional stacking-chip package layout on micro-void formation during encapsulation process”, *Microelectronics Reliability*, vol. 65, pp. 205-216, 2016.
- [2] A. A. Mohammad, “Lattice Boltzmann Method – Fundamentals and Engineering Applications with Computer Codes”, Springer, London, 2011. ISBN: 978-0-85729-455-5.
- [3] S. Succi, “The lattice Boltzmann equation for fluid dynamics and beyond”, Oxford University Press, Oxford, 2001.
- [4] S. Chen and G.D. Doolen, “Lattice Boltzmann method for fluid flows”, *Annual Review of Fluid Mechanics*, vol. 30, pp. 329–364, 1998.
- [5] M. Sukop and T. T. Daniel Jr, “Lattice Boltzmann Modelling – An Introduction for Geoscientists and Engineers”, Springer, Berlin, 2006.
- [6] D. P. Ziegler, “Boundary conditions for the lattice Boltzmann simulations”, *Journal of Statistical Physics*, vol. 71, no. 5-6, pp. 1171–1177, 1998.
- [7] Y. Liu, X. Guan and C. Xu, “A production limiter study of SST-SAS turbulence model for bluff body flows”, *Journal of Wind Engineering & Industrial Aerodynamics*, vol. 170, pp. 162–178, 2017.
- [8] D. T. Prosser and M. J. Smith, “Characterization of flow around rectangular bluff bodies at angle of attack”, *Physics Letters A*, vol. 376, pp. 3204–3207, 2012.
- [9] E. C. Joubert, T. M. Harms and G. Venter, “Computational simulation of the turbulent flow around a surface mounted rectangular prism”, *Journal of Wind Engineering and Industrial Aerodynamics*, vol. 142, pp. 173–187, 2015.
- [10] F. B. Teixeira, G. Lorenzini, M. R. Errera, L. A. O. Rocha, L. A. Isoldi and E. D. dos Santos, “Constructal Design of triangular arrangements of square bluff bodies under forced convective turbulent flows”, *International Journal of Heat and Mass Transfer*, vol. 126, pp. 521–535, 2018.
- [11] A. Cimarelli, A. Leonforte, D. Angeli, “Direct numerical simulation of the flow around a rectangular cylinder at a moderately high Reynolds number”, *Journal of Wind Engineering & Industrial Aerodynamics*, vol. 174, pp. 39–49, 2018.
- [12] F. Kawamura, Y. Seki, K. Iwamoto, H. Kawamura, “DNS of heat transfer in turbulent and transitional channel flow obstructed by rectangular prisms”, *International Journal of Heat and Fluid Flow*, vol. 28, pp. 1291–1301, 2007.
- [13] D. Rossinelli, M. Bergdorf, G. H. Cottet, P. Koumoutsakos, “GPU accelerated simulations of bluff body flows using vortex particle methods”, *Journal of Computational Physics*, vol. 229, pp. 3316–3333, 2010.
- [14] Ansys-Fluent 12.0, User’s Guide, Ansys Inc. 2019.
- [15] D. A. Perumal, G. V. S. Kumar, and A. K. Dass, “Numerical Simulation of Viscous Flow over a Square Cylinder Using Lattice Boltzmann Method,” *ISRN Mathematical Physics*, vol. 2012, Article ID 630801, 16 pages, 2012.
- [16] S. U. Islam, C. Y. Zhou, A. Shah, “Numerical simulation of flow past rectangular cylinders with different aspect ratios using the incompressible lattice Boltzmann method”, *Journal of Mechanical*

Science and Technology, vol. 26 no. 4, pp. 1027-1041, 2012.

- [17] M. A. Moussaoui, A. Mezrhab, H. Naji, and M. E. Ganaoui, “Prediction of heat transfer in a plane channel built-in three heated square obstacles using an MRT lattice Boltzmann method”, Proc. 6th Int. Conf. on Computational Heat and Mass Transfer, Guangzhou, pp. 176–181, 2009.
- [18] P. Bhatnagar, E. Gross, and M. Krook, “A model for collisional processes in gases I: Small amplitude processes in charged and neutral one-component system”, Physical Review, vol. 94, pp. 511–525, 1954.
- [19] X. He and L. S. Luo, “Lattice Boltzmann model for the incompressible Navier–Stokes equation”, Journal of Statistical Physics, vol. 88, pp. 927–944, 1997.
- [20] R.I. Issa, “Solution of the implicitly discretised fluid flow equations by operator splitting”, Journal of Computational Physics vol. 62, pp. 40–65, 1996.
- [21] A. Bejan, Heat Transfer, New York: John Wiley & Sons, 1993.